Chapter 3

AlAs/$In_{0.53}Ga_{0.47}As$ Double Barrier Resonant Tunneling Diodes (DBRTDs)

In this chapter we will briefly describe the operation of DBRTDs and their potential application at very high frequencies. It will be shown why AlAs/$In_{0.53}Ga_{0.47}As$ rather than AlAs/GaAs or AlSb/InAs is the material system of choice for obtaining increased ΔJ, the available current density. The effect of varying the AlAs/$In_{0.53}Ga_{0.47}As$ DBRTD barrier thickness on the J - V characteristics will also be discussed.

3.1 Introduction

Electron tunneling through multiple barriers has been studied since the advent of quantum mechanics. The Kronig-Penny model, published in 1930, describes the coherent interaction of an electron with a one dimensional periodic potential. An electron experiencing such a periodic potential can have only certain allowed energy values separated by forbidden energy gaps [1]. Two decades later, David Bohm in his textbook, "Quantum Theory," solved the double barrier problem in the WKB approximation and pointed out that resonances in the transmission coefficient occur for certain incident electron energies [2]. However, it remained a textbook problem until the early 1960's when it was realized that this phenomenon could be observed in a mesoscopic man-made device. Davis and Hosack in 1963 analyzed the electron transmission coefficient of a thin-film triode that was modeled as a double barrier with the third contact applied to a layer between the double barrier layers [3]. This structure was the forerunner of the present resonant tunneling transistor [4]. In an independent effort, Iogansen in the Soviet Union published a paper in 1964 pointing out the possibility of resonant transmission of electrons through double barriers formed from semiconductor crystals [5]. Then, in the early 1970's, R. Tsu and L. Esaki computed the two-terminal I - V characteristics of a finite superlattice with the transfer matrix method of Kane. They showed that resonances are observable not only in the transmission coefficient but also in the I - V characteristics [6]. They confirmed their calculations in 1974 by demonstrating resonant tunneling of electrons in MBE grown double barrier structures consisting of a thin GaAs well between

AlGaAs barriers [7]. The resonances were observed at liquid nitrogen temperatures as peaks and inflections in the I - V characteristics at voltages corresponding to the energy of the quasi-bound states in the quantum well.

However the field lay dormant until 1983 when Sollner *et al.* demonstrated radio frequency (RF) detection and mixing at frequencies up to 2.5 THz with $Al_{0.25}Ga_{0.75}As$/GaAs DBRTDs [8]. Such high frequency operation implied that the intrinsic charge transport mechanism in these devices was on the order of hundreds of femtoseconds. These results created a surge of interest in DBRTDs as potential high frequency sources at millimeter and sub-millimeter wavelengths and as ultra-fast logic elements. DBRTD oscillators soon followed [9] and worldwide efforts to develop high frequency DBRTDs were initiated. Advances in DBRTDs and quantum-effect devices, in general, have resulted from improvements in epitaxial growth technology, in particular, MBE and MOCVD.

The study of the phenomenon of resonant tunneling is now a vast discipline with many sub fields. The DBRTD has been investigated extensively both as a tool for studying physical processes in semiconductor heterostructures and for ultra-high speed device applications. From a fundamental physics aspect, various physical phenomena such as hot-electron transport, localization and quantum interference effects, scattering at hetero-interfaces, and tunneling through barriers can be studied with DBRTDs [10]. This work, however, focuses on the application of DBRTDs as high frequency oscillators. We will begin with a brief review of the physical principles of operation of DBRTDs.

The conduction energy band profile in a AlAs/GaAs DBRTD is shown in Fig. 3.1(a). Due to the thin GaAs layer, quantum size effects result in the formation of a quasi-bound state at energy E_o [11]. If the barriers are thin enough, then an electron with this energy can resonantly tunnel from one electrode through the well to the other electrode. As illustrated in Fig. 3.1(b), as the voltage is increased, electrons from the degenerately doped emitter electrode tunnel through the quantum well into an empty state in the collector electrode. As the voltage is increased further, the current increases until the emitter conduction band edge sweeps past the quasi-bound state. Once the peak current is reached, applying further voltage will move the emitter conduction band edge above the quasi-bound state and the current will drop (Fig. 3.1(c)) as the electron transmission through the quantum well is reduced. This phenomenon gives rise to negative differential resistance (NDR) in

the I - V curve as shown in Fig. 3.1(d). The current will eventually rise again with further applied voltage. The physical mechanisms causing this post-valley current are difficult to represent in the simple picture of Fig. 3.1 and are related to complex bandstructure effects. This point will be discussed in further detail later in this chapter.

Assuming that the applied voltage drops uniformly across the quantum well region only and neglecting any parasitic series resistance, the peak voltage will be equal to $2E_o/q$ as shown in Fig. 3.1 (d). This is due to the fact that an applied bias of E_o/q will bring the emitter Fermi level only half-way up to E_o since the voltage is dropped equally across each barrier. This assumption is valid only if the heavily doped contact layers are immediately adjacent to the quantum well. In DBRTD oscillator diodes, however, a significant fraction of the applied voltage is dropped across the spacer layers outside the quantum well. In fact, in chapter 4, we will see how a judicious choice of spacer layer profiles can significantly enhance the DBRTD oscillator diode output power.

The salient points of interest in Fig. 3.1 (d) are the peak current density, J_p, the valley current density, J_v, the peak voltage, V_p, and the valley voltage, V_v. Figures of merit for high speed DBRTDs are the J_p and peak-to-valley-current ratio (PVCR) and they should be as large as possible.

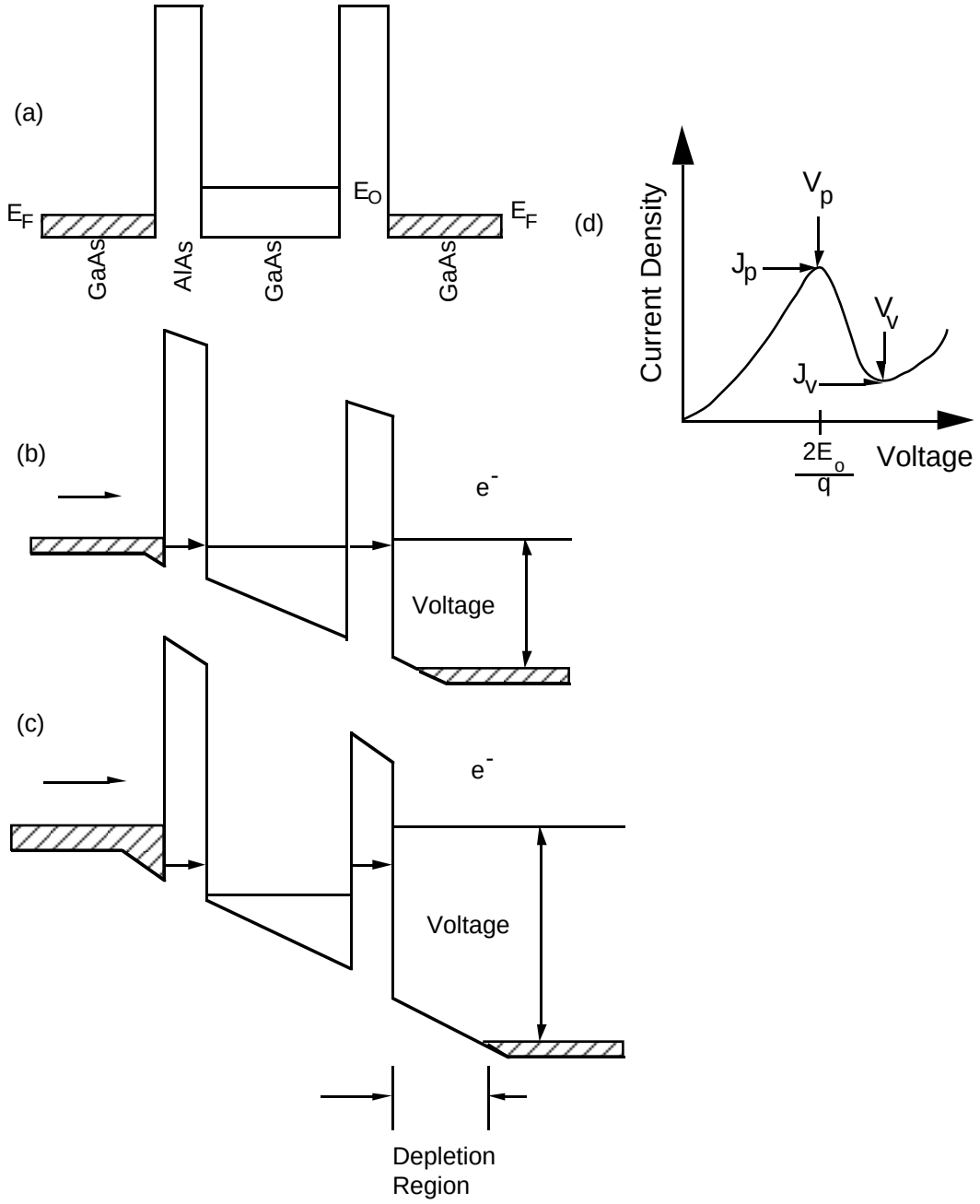

Fig. 3.1 Conduction band-edge profile of DBRTD at (a) equilibrium (b) at resonance (c) off-resonance (d) I - V characteristic showing NDR. Adapted from Sollner et al., Appl. Phys. Lett., vol. 43, No. 6, pp.588-590, 1983.

3.2 Self-consistent Schrodinger/Poisson DBRTD Simulation

To accurately calculate the DBRTD I - V characteristics, space charge effects must be incorporated by self-consistently solving Poisson's equation with the electron concentration calculated with Schrodinger's equation [12]. We begin by assuming that the DBRTD is described by the following single particle Hamiltonian [13]

$$H = -\frac{h^2}{8\pi^2 m^*}\frac{\partial^2}{\partial z^2} + v(z) \tag{3.1}$$

where m* is a position independent effective mass, v(z) includes the self-consistent Hartree potential and any conduction band offsets in the device, and *h* is Planck's constant. The simulation domain is discretized in space and the electron concentration at the grid point j is

$$n_j = \frac{4\pi m^* k_B T}{h^2}\left[\int_{V_L}^{\infty}\frac{dE}{hs_L(E)}\ln\left(1+e^{-(E-\mu L)/kBT}\right)\psi_{L,j}(E)\psi^*_{L,j}(E) + \int_{V_R}^{\infty}\frac{dE}{hs_R(E)}\ln\left(1+e^{-(E-\mu R)/kBT}\right)\psi_{R,j}(E)\psi^*_{R,j}(E)\right] \tag{3.2}$$

where the subscripts R and L (right and left) on the wave functions ψ denote the contacts with which the corresponding states are in equilibrium, *s* and μ are the electron group velocity and chemical potential respectively, and the subscripts R and L denote the contacts where they are defined. The complex wave function ψ corresponding to the energy E is obtained by solving the set of difference equations

$$H\psi_j = -\frac{1}{2m^*\Delta_Z^2}\psi_{j-1} + \left(\frac{1}{m^*\Delta_Z^2} + v_j\right)\psi_j - \frac{1}{2m^*\Delta_Z^2}\psi_{j+1} = E\psi_j \tag{3.3}$$

At each energy E in the domain of integration in Eq. (3.2), the set of equations in Eq. (3.3) is augmented with quantum transmitting boundary conditions [14]. The modification of the electrostatic potential due to the electron density computed above is then calculated by solving Poisson's equation between the two contacts:

$$\frac{d}{dz}\left(\varepsilon(z)\frac{d}{dz}(-V(z))\right) = q\left[N_D^+(z) - n(z)\right] \tag{3.4}$$

The Schrödinger and Poisson equations are solved iteratively until self-consistency is achieved. Finally the current through the device is calculated using the Esaki-Tsu like expression:

$$J = \frac{qm_c^*}{2\pi^2\hbar^3}\int dE_l \int dE_t\, T(E,E_t)\left[f_L(E) - f_R(E+qV)\right] \tag{3.5}$$

where E_l and E_t are, respectively, the longitudinal and transverse component of the electron total energy E; $f_L(E)$ and $f_R(E)$ are, respectively, the Fermi-Dirac distribution function in the left and right contacts; V is the bias applied across the structure, m_c is the electron effective mass in the contact; and $T(E,E_t)$ is the electron transmission coefficient.

Shown in Fig. 3.2 is a plot of the equilibrium electron transmission coefficient, $T(E,E_t)$, and conduction energy band diagram for a baseline AlAs/$In_{0.53}Ga_{0.47}As$ DBRTD, whose quantum well consists of a 50Å $In_{0.53}Ga_{0.47}As$ layer sandwiched between 17Å AlAs barriers. Clearly seen are the extremely sharp resonances of the two peaks, which correspond to the first and second quasi-bound states. The first quasi-bound state energy, E_o, is 145 meV above the $In_{0.53}Ga_{0.47}As$ quantum well conduction band edge.

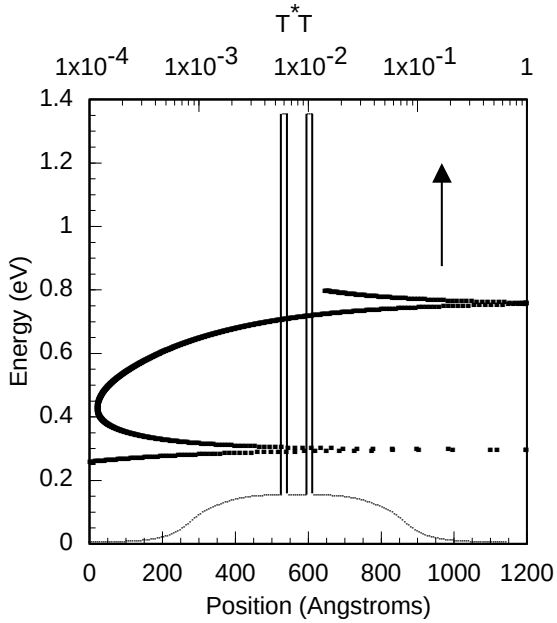

Fig. 3.2 Transmission coefficient and conduction band diagram for AlAs/$In_{0.53}Ga_{0.47}As$ DBRTD at equilibrium. Plot provided by K. Gullapalli.

The calculated J - V characteristic of the same structure is shown in Fig. 3.3 with V_p and J_p equal to 0.8 V and 130 kA/cm^2, respectively. The measured J - V characteristic is given in Fig. 4.6 and the measured V_p and J_p are 1.0 V and 95 kA/cm^2, respectively. Note that $2E_o/q$ for this structure is only 0.29 V. Therefore, a significant fraction of the applied voltage is dropped across the spacer layers in the downstream depletion region and upstream accumulation region. The electron effective mass used in the AlAs barrier that provided the closest match to experimental data was $0.12m_o$, which is lower than the bulk AlAs Γ-point electron effective mass of $0.15m_o$. The calculated peak current density is a strong function of the electron effective mass, which should be considered a fitting parameter. For example, reducing the AlAs effective mass to $0.08m_o$ results in a calculated peak current density of 250 kA/cm^2, a factor of two greater than the case when m_{AlAs} equals $0.12m_o$.

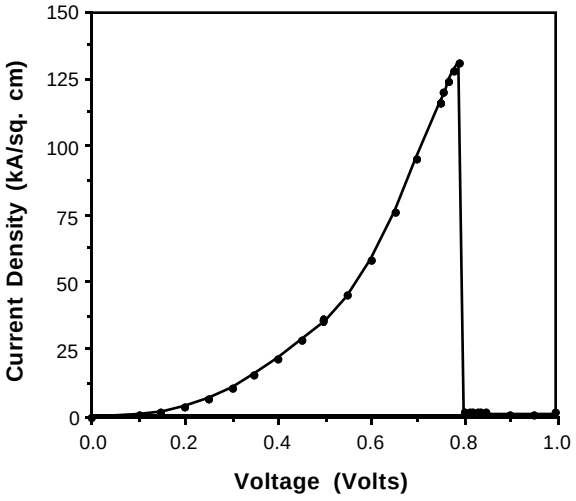

Fig. 3.3 Self-consistent Schrodinger/Poisson calculation of J - V characteristic of AlAs/$In_{0.53}Ga_{0.47}As$ DBRTD. Plot provided by K. Gullapalli.

A further point to be noted is that the PVCR calculated with the self-consistent Schrodinger-Poisson solver is about 145, which is a factor of fifteen greater than the measured PVCR. This large disparity is due to the fact that realistic band structure effects (i.e., multiple valleys, non-parabolicity, multiple bands, etc.) and phonon and impurity scattering have not been considered. To accurately calculate J - V characterisitcs and incorporate these effects, quantum kinetic approaches based, for example, on the Lattice Wigner function must be employed [15]. These techniques, however, are in their initial stages of development and extremely computationally intensive and application to realistic devices is very limited. Although the PVCR can not be accurately calculated with the self-consistent Schrodinger-Poisson technique, it is nevertheless quite useful as a device design tool since the peak voltage and peak current density can be calculated quite accurately and rapidly.

3.3 DBRTDs as high frequency devices

The potential for high speed operation of tunneling devices can be seen by representing the device with the parallel RC equivalent circuit shown in Fig. 3.4.

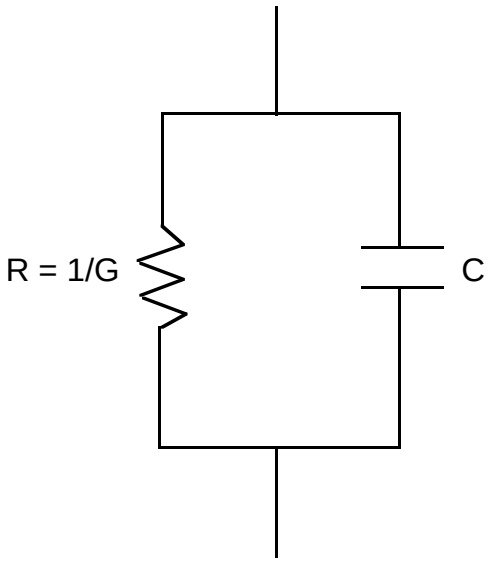

Fig. 3.4 Parallel RC equivalent circuit of intrinsic tunneling diode neglecting any parasitic series resistance.

If the device length, L, is thin enough and the carrier transport is dominated by tunneling, it is reasonable to expect an exponential dependence of R on L. The device's RC time constant, τ, then scales with L as follows

$$\tau = RC = C\frac{1}{G} \;\alpha\; \frac{1}{L}\frac{1}{e^{\lambda/L}} \;\alpha\; \frac{e^{-\lambda/L}}{L} \tag{3.6}$$

where λ is a proportionality constant relating the conductance to the device length. Thus as L is reduced τ decreases exponentially with a corresponding increase in the frequency response. In DBRTDs and p-n junction tunnel diodes, L is typically 100Å or less. Consequently, tunneling devices are expected to have very high frequency response since the conductance is high enough to prevent the shunt capacitance from dominating the device characteristics until the very highest frequencies are reached. DBRTDs offer a significant advantage over p-n junction

tunnel diodes since much higher conductances and lower capacitances can be achieved. Furthermore, the p-n junction tunnel diode I - V characteristics are essentially limited by the material properties, whereas DBRTDs can be engineered by varying the quantum well dimensions and material properties with MBE.

The high speed properties of DBRTDs have found recent use in switching and trigger circuits. Ozbay et al. have measured DBRTD switching times as low as 1.7 ps, the fastest switching time reported for any semiconductor device [16]. They have also demonstrated 110 GHz trigger circuits by monolithically integrating DBRTDs into coplanar transmission lines [17]. However, the surge of interest in DBRTDs was originally due to their promise as oscillators and not as logic elements. The inherent NDR observed in the I - V characteristic and the rapid tunneling transport mechanism make DBRTDs attractive candidates for high frequency (greater than 100 GHz) oscillator applications.

A further advantage of DBRTDs over p-n junction tunnel diodes is that the voltage and current scales are much larger in DBRTDs. Therefore, much larger RF output powers can be obtained. This can be understood if one considers Fig. 3.5 where the device is biased in the middle of the NDR region and a sinusoidal voltage is applied to the device. The RF output power density is then, in the low frequency limit, proportional to the $\Delta V \Delta J$ product. Therefore, to increase the RF output power, the $\Delta V \Delta J$ power density product must be maximized. The optimization of the $\Delta V \Delta J$ power density product is the subject of the rest of chapter 3 and chapter 4.

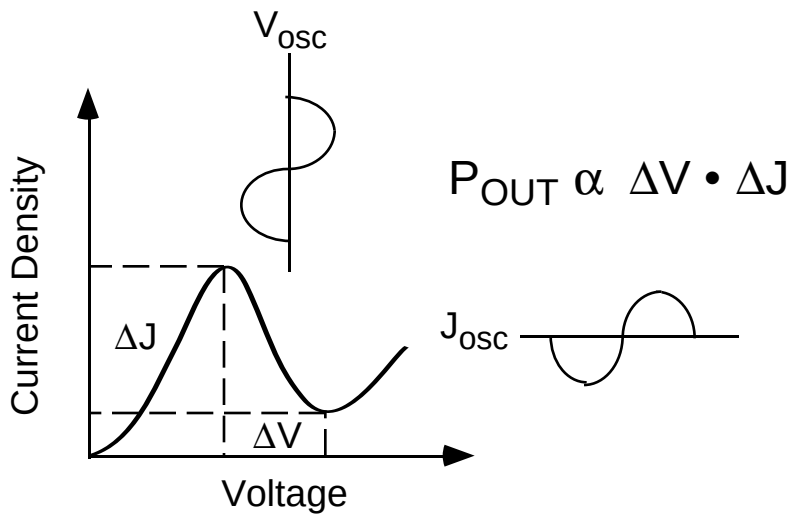

Fig. 3.5 When DBRTD is biased in the NDR region and a sinusoidal voltage is applied across the device as shown, the RF output power density is proportional to the ΔV•ΔJ product.

3.4 AlAs/$In_{0.53}Ga_{0.47}As$: Material system of choice

To increase the RF output power both ΔV and ΔJ must be increased. We will see in the next chapter that by adding a moderately thick spacer layer of the appropriate length, one can increase the ΔV over that of a baseline DBRTD. To increase ΔJ, one must increase the peak current density as ΔJ is given by the following relation

$$\Delta J = J_p\left(1 - \frac{1}{PVCR}\right) \tag{3.7}$$

However, in the AlAs/GaAs material system, as one reduces the barrier thickness, the PVCR suffers and ΔJ does not increase as rapidly as one would expect. For example, AlAs/GaAs DBRTDs with 14Å (5 monolayer (ML)) AlAs barriers and 50Å (18 ML) GaAs quantum well have peak current densities as high as 250

kA/cm^2 but the ΔJ is 110 kA/cm^2 since the PVCR is only 1.8 [18]. The reduction in PVCR can be understood by examining Fig. 3.6 which illustrates the AlAs/GaAs conduction band structure with the X-point band edge in bold and the Γ-point band edge in the thin line. For the AlAs/GaAs heterojunction, the $\Delta E_{\Gamma\Gamma}$ and $\Delta E_{\Gamma X}$ barrier heights are 1.05 eV and 0.20 eV, respectively [19]. Also shown is the Γ-X valley separation in GaAs, which is approximately 0.48 eV.

Since the Γ_{GaAs} - X_{AlAs} barrier is much lower than the Γ_{GaAs} - Γ_{AlAs} barrier, it is expected that the smaller $\Delta E_{\Gamma X}$ barrier height will play a significant role in carrier transport. In fact, it is now well established that the small $\Delta E_{\Gamma X}$ barrier tunneling is a dominant component of the valley current in AlAs/GaAs DBRTDs [20]. The valley current dependence on the $\Delta E_{\Gamma X}$ barrier has been confirmed by many workers through hydrostatic pressure experiments.

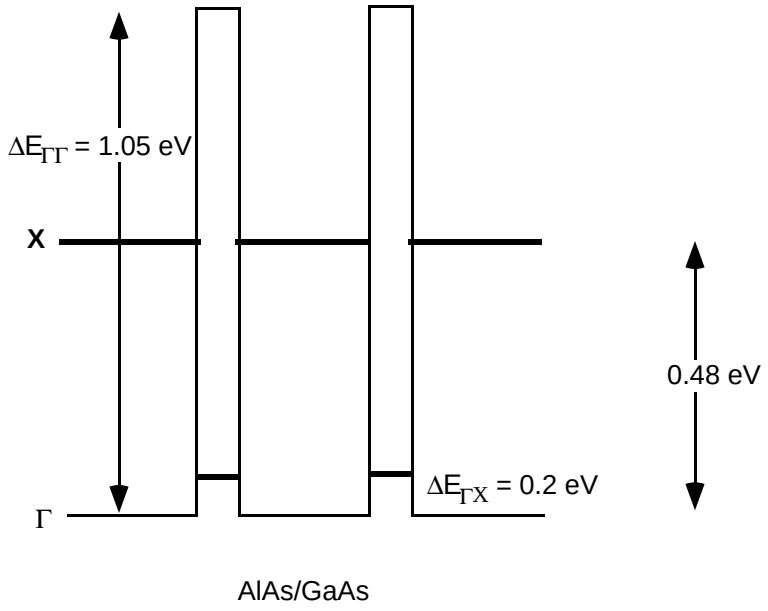

Fig. 3.6 Conduction band edge profile for AlAs/GaAs DBRTDs showing both the $\Delta E_{\Gamma\Gamma}$ (1.05 eV) and $\Delta E_{\Gamma X}$ (0.20 eV) barrier heights. Also shown is the Γ-X valley separation in GaAs (0.48 eV).

These experiments involve measuring the DBRTD J - V characteristics as a function of hydrostatic pressure. This technique relies on the fact that $\Delta E_{\Gamma X}$ barrier height varies strongly with pressure, decreasing at a rate of 11 meV/kbar, while the $\Delta E_{\Gamma\Gamma}$ barrier height is essentially independent of the applied pressure [21]. Using this approach, Mendez *et al.* have shown that the resonant tunneling current, which is the dominant component of the peak current, is determined by the Γ-Γ band profile [22]. Their results also indicate that non-resonant tunneling current occurs primarily through the lowest barrier, the $\Delta E_{\Gamma X}$ barrier. The valley current due to this non-resonant or inelastic tunneling current, is composed of phonon-coupled and impurity-assisted tunneling components [23]. The ratio of the resonant to the non-resonant tunneling current determines the PVCR and has been shown to influenced by the AlAs barrier width. Kyono *et al.* have conducted temperature dependent I - V measurements on single barrier AlAs/GaAs diodes in which they varied the barrier width from 14.2Å to 150Å [24]. Their measurements indicate that elastic tunneling dominates for very thin (14.2Å) AlAs barriers while thermionic emission is the primary transport mechanism in thick (150Å) AlAs barriers. The current in the intermediate thickness range, however, appears to consist of both elastic tunneling and inelastic tunneling components through the Γ_{GaAs} - X_{AlAs} barrier.

A thorough investigation of the pressure dependence of X-point and Γ-point related tunneling resonances in AlAs/GaAs DBRTDs has recently been conducted by Austing *et al.* [25]. They show that for AlAs barriers 30Å and thicker, hydrostatic pressure reduces the PVCR significantly and with high enough pressure the NDR completely disappears. The AlAs barrier thicknesses discussed in our work are thinner (14Å to 20Å) and the current transport mechanism contributing to the peak current is Γ-point dominated. However, the valley current definitely has a strong X-point related tunneling component. In fact, Cheng *et al.* reported improved PVCR in AlAs/GaAs DBRTDs which utilized a four monolayer $Al_{0.14}Ga_{0.86}As$ "chair" barrier adjacent to one of the AlAs barriers [26]. They attributed the improved PVCR to a reduction in the resonant tunneling and X-point

mediated tunneling components of the valley current. We have also fabricated AlAs/GaAs DBRTDs with a four monolayer $Al_{0.2}Ga_{0.8}As$ chair barrier adjacent to one of the AlAs barriers and have achieved a PVCR of 6.3 [27]. This is the highest reported PVCR at room temperature for AlGaAs/GaAs DBRTDs and the reader is referred to Alwin Tsao's Ph.D. dissertation for further details [28]. Although, the chair barrier approach does result in a higher PVCR, it does so at the expense of reduced J_p and ΔJ, since the chair barrier results in an effectively thicker barrier. Another approach to increasing the J_p and PVCR in AlAs/GaAs DBRTDs has been to insert a pseudomorphic $In_{0.15}Ga_{0.85}As$ "pre-well" adjacent to one of the AlAs barriers, resulting in a PVCR of 7.2 at room temperature but with a J_p of only 10 kA/cm^2 [29]. Recently, Yang *et al.* demonstrated AlAs/GaAs DBRTDs with a linearly graded AlGaAs layer adjacent to the AlAs barrier [30]. The purpose of this graded layer was to reduce the hump in the conduction band that is caused by space charge effects in the spacer layers used in conventional structures. By incorporating this graded AlGaAs layer, they achieved a J_p of 170 kA/cm^2 with a PVCR of 3.2 (ΔJ = 170 kA/cm^2). Although this is quite an impressive result for GaAs based DBRTDs, higher performance can be achieved with AlAs/$In_{0.53}Ga_{0.47}As$ DBRTDs as will be shown later. Furthermore, reproducible MBE growth of the graded AlGaAs layer required in such a structure is difficult and variations in the grading will have significant impact on the J - V characteristics.

The above discussion illustrates the importance of X-point related transport in AlAs/GaAs DBRTDs and suggests that higher performance (higher J_p without sacrificing PVCR) can be achieved if the $\Delta E_{\Gamma X}$ barrier height can be increased. Such an increase is possible if the quantum well material system is changed to the AlAs/$In_{0.53}Ga_{0.47}As$ material system. The conduction band edge for the AlAs/$In_{0.53}Ga_{0.47}As$ system is shown in Fig. 3.7 where the $\Delta E_{\Gamma\Gamma}$ and $\Delta E_{\Gamma X}$ barrier heights are 1.2 eV and 0.65 eV, respectively [27]. The Γ-X valley separation in $In_{0.53}Ga_{0.47}As$, approximately 1.05 eV, is much higher than in GaAs [31].

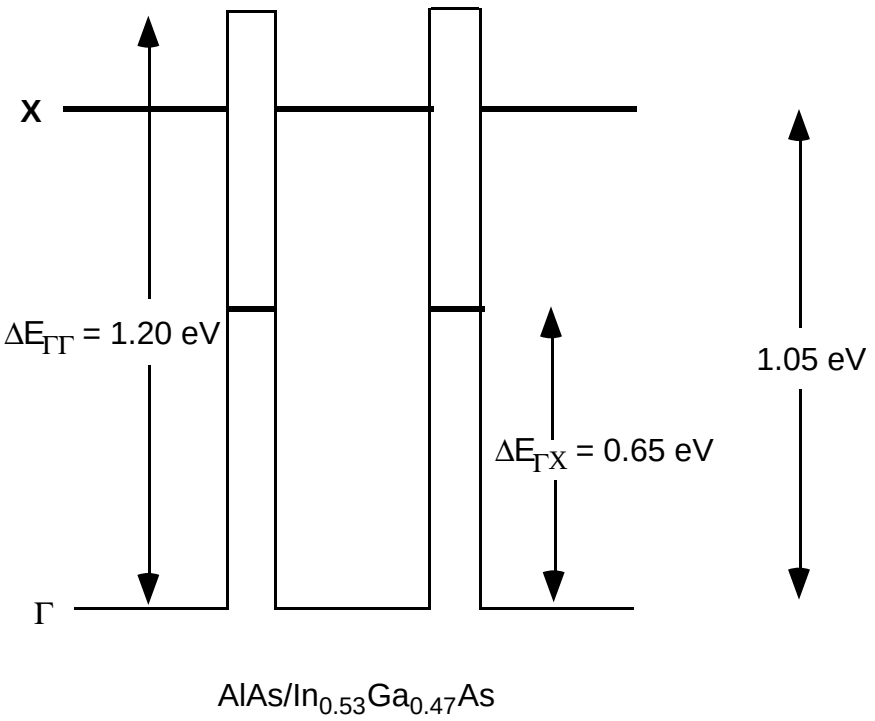

Fig. 3.7 Conduction band edge profile for AlAs/$In_{0.53}Ga_{0.47}As$ DBRTDs showing both the $\Delta E_{\Gamma\Gamma}$ (1.2 eV) and $\Delta E_{\Gamma X}$ (0.65 eV) barrier heights. Also shown is the Γ-X valley separation in GaAs (1.05 eV).

Comparing the two conduction band profiles in Figs. 3.6 and 3.7, one sees that while the $\Delta E_{\Gamma\Gamma}$ barrier heights are similar, the $\Delta E_{\Gamma X}$ barrier height is much higher in the AlAs/$In_{0.53}Ga_{0.47}As$ material system. Therefore, this material system should be superior to the AlAs/GaAs material system since the parasitic Γ-X mediated transport will be reduced.

Inata *et al.* were the first to study AlAs/$In_{0.53}Ga_{0.47}As$ DBRTDs and they observed that for a given J_p, a higher PVCR could be achieved with AlAs/$In_{0.53}Ga_{0.47}As$ DBRTDs than with AlAs/GaAs DBRTDs [32]. Interest in this material system grew when Broekaert *et al.* reported AlAs/$In_{0.53}Ga_{0.47}As$/InAs DBRTDs with PVCRs as high as 30 at room temperature [33]. The AlAs barriers in these devices were ten monolayers thick and J_p was quite low, about 5 kA/cm^2.

Nevertheless, this result generated interest since, at the time, that was the highest PVCR ever reported for DBRTDs. Then, Broekaert *et al*. reported AlAs/$In_{0.53}Ga_{0.47}As$ DBRTDs with peak current densities as high as 460 kA/cm^2 with a PVCR of 4 [34]. This results in a ΔJ of 345 kA/cm^2, which is the highest ΔJ reported in any material system. To achieve such high J_p, extremely thin (four ML) AlAs barriers and a 16 ML $In_{0.53}Ga_{0.47}As$ quantum well were employed. As a point of comparison, no AlAs/GaAs DBRTDs have been even reported with such high J_p. The above discussion makes clear that the AlAs/$In_{0.53}Ga_{0.47}As$ material system is the preferred system for high speed oscillator applications since both high J_p and PVCR DBRTDs can be fabricated.

3.5 AlAs/$In_{0.53}Ga_{0.47}As$ DBRTDs: barrier thickness dependence

This section discusses the barrier thickness dependence of the J - V characteristics of thin barrier AlAs/$In_{0.53}Ga_{0.47}As$ DBRTDs. AlAs/$In_{0.53}Ga_{0.47}As$ DBRTDs with barrier thicknesses of 5, 6, and 7 monolayers were fabricated and tested. The layer schematic of the devices is shown in Fig. 3.8. Sulfur doped (n = 3 x 10^{18} c m^{-3}) liquid encapsulated Czochralski grown InP substrates from Sumitomo Chemical were used. Heavily doped (n = 2.2 x 10^{19} cm^{-3}), 2000Å thick top and bottom buffer $In_{0.53}Ga_{0.47}As$ layers were employed as contact cladding layers. The quantum well is sandwiched between a three-step dopant transition region consisting of 100Å (n = 6.0 x 10^{17} cm^{-3}) $In_{0.53}Ga_{0.47}As$, 100Å (n = 4.3 x 10^{16} cm^{-3}) $In_{0.53}Ga_{0.47}As$, and finally 50Å of nominally undoped (n = 5 x 10^{15} cm^{-3}) $In_{0.53}Ga_{0.47}As$ adjacent to the AlAs barrier. The quantum well consists of a 50Å nominally undoped $In_{0.53}Ga_{0.47}As$ quantum well and pseudomorphic AlAs barriers. No growth interruption at the hetero-interfaces was used. The device fabrication process and electrical test procedure are given in Appendix 1.

2000Å	2.2 x 10^{19} cm^{-3}	InGaAs
100Å	6.0 x 10^{17} cm^{-3}	InGaAs
100Å	4.3 x 10^{16} cm^{-3}	InGaAs
50Å	Undoped	InGaAs
L	Undoped	AlAs
50Å	Undoped	InGaAs
L	Undoped	AlAs
50Å	Undoped	InGaAs
100Å	4.3 x 10^{16} cm^{-3}	InGaAs
100Å	6.0 x 10^{17} cm^{-3}	InGaAs
2000Å	2.2 x 10^{19} cm^{-3}	InGaAs
	n+ InP substrate	

Fig. 3.8 Layer schematic of AlAs/$In_{0.53}Ga_{0.47}As$ DBRTDs to study the barrier thickness dependence on the J - V characteristics. The quantum well consists of a 50Å $In_{0.53}Ga_{0.47}As$ layer sandwiched between pseudomorphic AlAs layers of thickness L. Three devices with L = 5, 6, and 7 ML barriers were studied.

Shown in Fig. 3.9 are measured J - V characteristics of the three devices. One can see the dramatic effect that the barrier thickness has on the J - V characteristics. Decreasing the barrier thickness by one monolayer approximately doubles the peak current density.

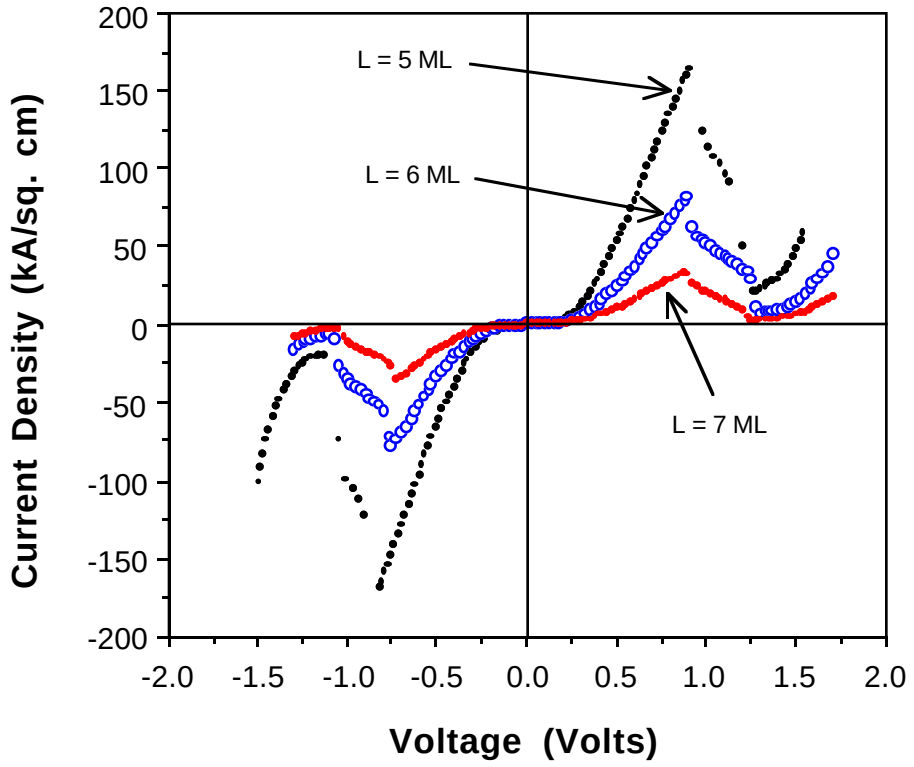

Fig. 3.10 Measured J - V characteristics of AlAs/$In_{0.53}Ga_{0.47}As$ DBRTDs with AlAs barrier thicknesses of 5, 6, and 7 ML. The voltage across the 5 ML AlAs barrier DBRTD is corrected for the ohmic contact resistance (ρ_c = 10^{-6} ohm-cm^2) since the very high peak current density (J_p ~ 165 kA/cm^2) magnifies the ohmic contact resistance effect. This correction results in a reduction of V_p of roughly 0.16 V and a corresponding increase in ΔV. Decreasing the barrier thickness by one monolayer increases the current density by roughly 100%.

Shown in Table 3.1 are values for the device parameters of interest for the devices shown in Fig. 3.9. These devices also show an asymmetry in the J - V characteristics similar to that seen in AlAs/GaAs DBRTDs. Namely, one observes a higher J_p and lower PVCR for forward bias (electron injection from the substrate), whereas for reverse bias, the PVCR is higher and the J_p is lower. The quantum well injection conductance (to be discussed in Chapter 4), extracted from the J - V characteristics, for the L= 5, 6, and 7 ML samples are - 1.3, -0.5, and -0.3 (ohm - cm)$^{-1}$, respectively.

Device Parameter	L=5ML For. Bias	Rev. Bias	L=6 ML For. Bias	Rev. Bias	L=7 ML For. Bias	Rev. Bias
J_p (kA/cm^2)	167	166	82	78	35	35
ΔJ (kA/cm^2)	146	148	74	72	32	33
PVCR	7.8	9.2	10.1	13	11.4	14.1
V_p	0.92	0.88	0.91	0.76	0.86	0.75
ΔV	0.36	0.27	0.4	0.35	0.39	0.33

Table 3.1 Typical device parameter values for AlAs/$In_{0.53}Ga_{0.47}As$ DBRTDs with 50Å $In_{0.53}Ga_{0.47}As$ quantum well and barrier thickness of 5, 6, and 7 ML.

The peak and valley current density as a function of barrier thickness are plotted in a semi-log plot in Fig. 3.10. This figure clearly shows the exponential dependence on barrier thickness that one would expect from Eq. 3.6 where the conductance is exponentially dependent on the barrier thickness.

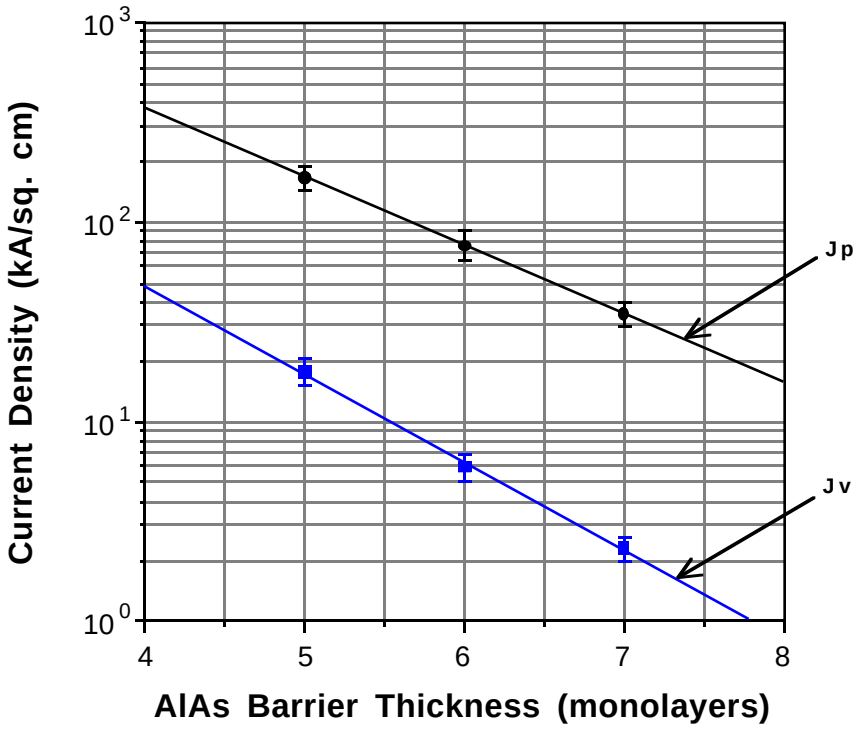

Fig. 3.10 Semi-log plot of J_p and J_v as a function of AlAs barrier thickness. The characteristics show the expected exponential dependence on the barrier thickness. The error bars denote a 10% uncertainty in device area measurement.

This exponential dependence has also been observed by Broekaert *et al.* [35] and Chow *et al.* [36]. If we model the exponential dependence of the peak current density as

$$J_p \alpha \exp\left(-\frac{L_B}{\lambda}\right) \tag{3.8}$$

where L_B is the barrier thickness in ML and λ is a characteristic length, we find that λ = 1.3 ML. This indicates that a variation in the barrier thickness on the order of a

one monolayer will result in the current density changing by a factor of two. Therefore, very tight control of the layer thicknesses is required and the techniques to achieve this level of control have been discussed in the previous chapter.

3.6 Comparison of Material Systems

For DBRTDs to generate useful amounts of output power at very high frequencies, the ΔJ of the device should be as large as possible so as to maximize the $\Delta V \Delta J$ power density product. We have implied that the AlAs/$In_{0.53}Ga_{0.47}As$ material system is the system of choice for obtaining this increased ΔJ. This was based on the observation that for a given J_p, much higher PVCR are obtained in the AlAs/$In_{0.53}Ga_{0.47}As$ system than in the AlAs/GaAs system. The improved performance was attributed to the higher $\Delta E_{\Gamma X}$ barrier height available with the AlAs/$In_{0.53}Ga_{0.47}As$ system.

One question to be asked is whether the additional effort required to fabricate AlAs/$In_{0.53}Ga_{0.47}As$ devices is warranted. Furthermore, are there other material systems that provide performance better or equal to that of the AlAs/$In_{0.53}Ga_{0.47}As$ system? To answer these questions, we plot ΔJ versus J_p at 300K in Fig. 3.11 for DBRTDs fabricated in three material systems: AlAs/GaAs, AlAs/$In_{0.53}Ga_{0.47}As$, and AlSb/InAs. The AlAs/GaAs data was obtained from [27],[17], and [29]. The AlAs/$In_{0.53}Ga_{0.47}As$ data was from [32], [33], [34], [37], and from devices presented in this work. The AlSb/InAs data was obtained from Soderstrom *et al.* [38]. The AlSb/InAs system has been suggested as an alternative to the AlAs/GaAs and AlAs/$In_{0.53}Ga_{0.47}As$ system due to the very high conduction band offsets available: 1.8 eV for Γ-Γ barrier height and 1.35 eV for the Γ-X barrier (Γ-point to AlSb X-point) [39]. This is expected to reduce X-point mediated tunneling currents and consequently increase the PVCR.

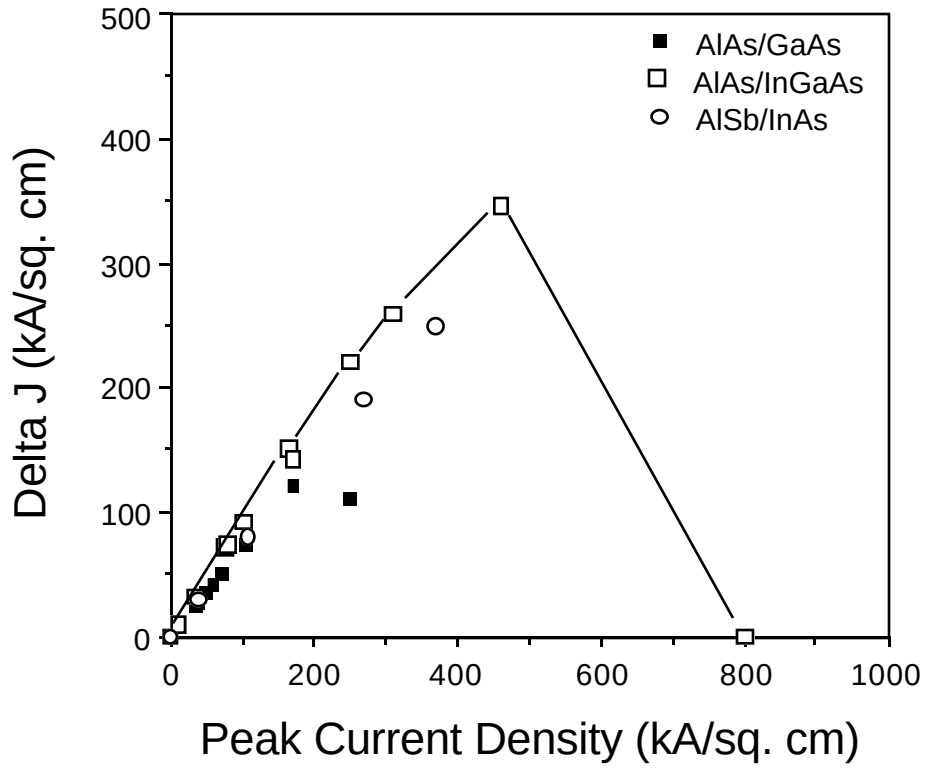

Fig. 3.11 Comparison of measured ΔJ vs J_p at 300K obtained with DBRTDs in the AlAs/GaAs, AlAs/$In_{0.53}Ga_{0.47}As$, and AlSb/InAs material systems.

Examining Fig. 3.11 we see that for small J_p (less than 50 kA/cm^2) all the points fall on top of each other and there is no significant difference in performance between the material systems. But as J_p is increased one begins to notice the performance difference between the material systems. The AlAs/GaAs devices achieve a maximum ΔJ of approximately 130 kA/cm^2 at a J_p of 200 kA/cm^2. Further increase in J_p results in reduced ΔJ since the PVCR begins to drop. The AlSb/InAs and the AlAs/$In_{0.53}Ga_{0.47}As$ DBRTDs offer a substantial performance advantage over AlAs/GaAs based devices with ΔJ's on the order of several hundred kA/cm^2. At a record high J_p of 800 kA/cm^2 (achieved with 3 ML AlAs barriers) the ΔJ of the AlAs/$In_{0.53}Ga_{0.47}As$ DBRTDs is essentially zero. This is due to the

fact that as the barrier thickness is reduced, the transmission coefficient changes to that of a single barrier with the consequent loss of NDR. Therefore, ΔJ will drop as the PVCR reduces (see Eq. 3.7). Nevertheless, it is apparent from Fig. 3.11 that the AlAs/$In_{0.53}Ga_{0.47}As$ devices are superior to the AlSb/InAs devices since they offer higher ΔJ's at very high J_p.

Returning to the questions posed at the beginning of this section, it is quite clear that the extra effort required for fabricating AlAs/$In_{0.53}Ga_{0.47}As$ devices is well worth the effort for very high frequency applications where large ΔJ is essential. Furthermore, from a device application perspective, AlSb/InAs DBRTDs may suffer from impact ionization events occurring in the very narrow band gap InAs (E_g @ 300K = 0.35 eV [40]). This is particularly true for high current density DBRTDs where electric fields on the order of several hundred kV/cm are encountered. This will be discussed further in chapters 4 and 5.

3.7 Summary

We have briefly described the operation of DBRTDs and their potential high speed applications. It was seen that increasing the $\Delta V \Delta J$ product will increase the DBRTD RF output power. The effect of varying the AlAs/$In_{0.53}Ga_{0.47}As$. DBRTD barrier thickness on the J - V characteristics was investigated. Precise control of layer thicknesses in DBRTDs is essential; since, changing the barrier thickness by one monolayer results in a factor of two change in the peak current density. We have also explained why AlAs/$In_{0.53}Ga_{0.47}As$ rather than AlAs/GaAs or AlSb/InAs is the material system of choice for obtaining increased ΔJ, the available current density.

References

[1] R. de L. Kronig and W. G. Penney, " Quantum Mechanics of Electrons in Crystal Lattices," Proceedings of the Royal Society, A130, p. 499, 1930.

[2] David Bohm, " Quantum Theory," Dover Books, New York, 1951.

[3] R. H. Davis and H. H. Hosack, " Double Barrier in Thin-Film Triodes," Journal of Applied Physics, vol. 34, No.4, pp.864-866, 1963.

[4] F. Capasso and R. A. Kiehl, " Resonant Tunneling Transistor with Quantum Well Base and High Energy Injection: A New Differential Resistance Device," J. Appl. Phys., vol. 58, p. 1366, 1985.

[5] L. V. Iogansen, " The possibility of resonance transmission of electrons in crystals through a system of barriers," Soviet Physics JETP, vol. 18, No. 1, pp.146-150, 1964.

[6] R. Tsu and L. Esaki, " Tunneling in a finite superlattice," Appl. Phys. Lett., vol. 22, No. 11, pp.562-564, 1973.

[7] L. L. Chang, L. Esaki, and R. Tsu, " Resonant tunneling in semiconductor double barriers," Appl. Phys. Lett., vol. 24, No. 12, pp.593-595, 1974.

[8] T. C. L. G. Sollner, W. D. Goodhue, P. E. Tannenwald, C. D. Parker, and D. D. Peck, " Resonant tunneling through quantum wells at frequencies up to 2.5 THz," Appl. Phys. Lett., vol. 43, No. 6, pp.588-590, 1983.

[9] T. C. L. G. Sollner, P. E. Tannenwald, D. D. Peck, and W. D. Goodhue, " Quantum Well Oscillators," Appl. Phys. Lett., vol. 45, No. 12, pp.1319-1321, 1984.

[10] L. L. Chang, E. E. Mendez, and C. Tejedor, Eds., " Resonant Tunneling in Semiconductors: Physics and Applications," Plenum Press, New York, 1991.

[11] Raymond Dingle, " Confined carrier quantum states in ultrathin semiconductor heterostructures," Festkorperprobleme XV, 1975.

[12] M. Cahay, M. McLennan, S. Datta, and M. S. Lundstrom, " Importance of space-charge effects in resonant tunneling devices," Appl. Phys. Lett., vol. 50, No. 10, pp.612-614, 1987.

[13] Kiran Kumar Gullapalli, Ph.D. Dissertation, May 1994.

[14] C. S. Lent and D. J. Kirkner, " The quantum transmitting boundary method," J. Appl Phys., vol. 67, No. 10, 1990.

[15] D. R. Miller, K. K. Gullapalli, V. K. Reddy, and D. P. Neikirk, " Simulation of Electron Transport in Quantum Well Devices," Proc. of the Third International Symposium on Space Terahertz Technology, March 24-26, pp.560-574, 1992.

[16] E. Ozbay, David. M. Bloom, D. H. Chow, and J. N. Schulman, " 1.7 ps, Microwave, Integrated-Circuit-Compatible InAs/AlSb Resonant Tunneling Diodes," IEEE Electron Device Lett., vol. 14, No. 8, pp.400-402, 1993.

[17] E. Ozbay and David M. Bloom, " 110-GHz Monolithic Resonant-Tunneling-Diode Trigger Circuit," IEEE Electron Device Lett., vol. 12, No. 9, pp.480-482, 1991.

[18] E. Wolak, E. Ozbay, B. G. Park, S. K. Diamond, D. M. Bloom, and J. S. Harris, " The design of GaAs/AlAs resonant tunneling diodes with peak current

densities over 2 x 10^5 A/cm^2," J. Appl. Phys., vol. 69, No. 5, pp.3345-3350, 1991.

[19] Sadao Adachi, " GaAs, AlAs, AlxGa1-xAs: Material parameters for use in research and device applications," J. Appl. Phys., vol. 58, No. 3, pp.R1-R29, 1985.

[20] L. L. Chang, E E. Mendez, and C. Tejedor, eds., " Resonant Tunneling in Semiconductors: Physics and Applications," Plenum Press, New York, 1991.

[21] R. Pritchard, P. C. Klipstein, N. R. Couch, T. M. Kerr, J. S. Roberts, P. Mistry, B. Soylu, and W. M. Stobbs, " High-pressure studies of resonant tunneling in a graded parameter superlattice and in double barrier structures of GaAs/AlAs," Semiconductor Science and Technology, vol. 4, pp.754-764, 1989.

[22] E. E. Mendez, E. Cajella, and W. I. Wang, " Tunneling through indirect-gap semiconductor barriers," Phys. Rev. B, vol. 34, No. 8, pp.6026-6029, 1986.

[23] E. E. Mendez, E. Cajella, and W. I. Wang, " Inelastic tunneling in AlAs/GaAs heterostructures," Appl. Phys. Lett., vol. 53, No. 11, pp.977-979, 1988.

[24] C. Kyono, V. P. Kesan, D. P. Neikirk, C. M. Maziar, and B. G. Streetman, " Dependence of apparent barrier height on barrier thickness for perpendicular transport in AlAs/GaAs single-barrier structures grown by molecular beam epitaxy," Appl. Phys. Lett., vol. 54, No. 6, pp.549-551, 1989.

[25] D. G. Austing, P. C. Klipstein, A. W. Higgs, H. J. Hutchinson, G. W. Smith, J. S. Roberts, and G. Hill," X- and Γ- related tunneling resonances in GaAs/AlAs double-barrier structures at high pressure," Phys. Rev. B, vol. 47, No. 3, pp.1419-1433, 1993.

[26] P. Cheng and J. S. Harris, " Improved design of AlAs/GaAs resonant tunneling diodes," Appl. Phys. Lett., vol. 56, No. 17, pp.1676-1678, 1990.

[27] V. K. Reddy, A. J. Tsao, and D. P. Neikirk, " High peak-to-valley current ratio AlGaAs/AlAs/GaAs double barrier resonant tunneling diodes," Electronics Lett., vol. 26, No. 21, pp.1742-1744, 1990.

[28] A. J. Tsao, " Molecular beam epitaxial growth and fabrication of microwave and photonic devices for hybrid integration on alternative substrates, Ph.D. Dissertation, The University of Texas at Austin, 1993.

[29] H. Brugger, U. Meiners, C. Wolk, R. Deufel, A. Marten, M. Rossmanith, K. v. Klitzing, and R. Sauer, " Pseudomorphic two-dimensional electron-gas-emitter resonant tunneling devices," Microelectronic Engineering, vol. 15, pp.663-666, 1991.

[30] L. Yang, D. E. Mars, and M. R. T. Tan, " Effect of electron launcher structures on AlAs/GaAs double barrier resonant tunneling diodes," J. Appl. Phys., vol. 73, No. 5, pp.2540-2542, 1993.

[31] Massimo V. Fischetti, " Monte Carlo simulation of transport in technologically significant semiconductors of the diamond and zinc-blende structures - Part I: Homogeneous transport," IEEE Trans. on Electron Devices, vol. 38, No. 3, pp.634-649, 1991.

[32] T. Inata, S. Muto, Y. Nakata, S.Sasa, T. Fujii, and S. Hiyamizu, " A pseudomorphic $In_{0.53}Ga_{0.47}As$/AlAs resonant tunneling barrier with a peak-to-valley current ratio of 14 at room temperature," Japanese Journal of Applied Phys., vol. 26, No. 8, pp.L1332-L1334, 1987.

[33] T. P. E. Broekaert, W. Lee, and C. G. Fonstad, " Pseudomorphic $In_{0.53}Ga_{0.47}As$/AlAs/InAs resonant tunneling diodes with peak-to-valley current ratios of 30 at room temperature," Appl. Phys. Lett., vol. 53, No. 16, pp.1545-1547, 1988.

[34] T. P. E. Broekaert and C. G. Fonstad, " $In_{0.53}Ga_{0.47}As$/AlAs resonant tunneling diodes with peak current densities in excess of 450 kA/cm^2," J. Appl. Phys., vol. 68, No. 8, pp.4310-4312, 1990.

[35] T. P. E. Broekaert and C. G. Fonstad, " Extremely high current density, low peak voltage, pseudomorphic $In_{0.53}Ga_{0.47}As$/AlAs/InAs Resonant tunneling diodes," 1989 IEDM Technical Digest, pp.559-562, 1989.

[36] D. H. Chow, J. N. Schulman, E. Ozbay, and D. M. Bloom, " Investigation of $In_{0.53}Ga_{0.47}As$/AlAs/ resonant tunneling diodes for high speed switching," Appl. Phys. Lett., vol. 61, No. 14, pp. 1685-1687, 1992.

[37] E. R. Brown, C. D. Parker, A. R. Calawa, M. J. Manfra, T. C. L G. Sollner, C. L. Chen, S. W. Pang, and K. M. Molvar, " High-speed resonant-tunneling diodes made from the In0.53Ga0.47As/AlAs material system,: Proc. on High-Speed Electronics and Device Scaling, SPIE vol. 1288, pp. 122-135, 1990.

[38] J. R. Soderstrom, E. R. Brown, C. D. Parker, L. J. Mahoney, and T. C. McGill, " Growth and characterization of high current density, high-speed InAs/AlSb resonant tunneling diodes," Appl. Phys. lett., vol. 58, No. 3, pp.275-277, 1991.

[39] J. R. Soderstrom, D. H. Chow, and T. C. McGill, " InAs/AlSb Double-Barrier Structure with Large Peak-to-Valley Current Ratio: A Candidate for High-Frequency Microwave Devices," IEEE Electron Device Lett., vol. 11, No. 1, pp.27-

29, 1990.

[40] A. Cappy, B. Carnez, R. Fauquembergues, G. Salmer, and E. Constant, " Comparative Potential Performance of Si, GaAs, GaInAs, InAs Submicrometer-Gate FET's," IEEE Trans. on Electron Devices, vol. 27, No. 11, pp.2158-2160, 1980.